J of Nuclear Medicine Technology, first published online November 9, 2018 as doi:10.2967/jnmt.118.208835

The influence of minimal misalignment on the repeatability of PET images examined by the repositioning of point sources

<Short running foot line>

Point source alignment for repeatability

Akira Maebatake, MS[1)], Keishin Morita, MS[1)], Go Akamatsu, PhD[2)], Yuji Tsutsui, BS[3)], Kazuhiko Himuro[3)], Shingo Baba, MD, PhD[4)], Masayuki Sasaki, MD, PhD[1)]

1) Division of Medical Quantum Science, Department of Health Sciences, Graduate School of Medical Sciences, Kyushu University, Fukuoka, Japan
2) National Institute of Radiological Sciences, National Institutes for Quantum and Radiological Science and Technology, Chiba, Japan
3) Division of Radiology, Department of Medical Technology, Kyushu University Hospital, Fukuoka, Japan
4) Department of Clinical Radiology, Graduate School of Medical Sciences, Kyushu University, Fukuoka, Japan

Corresponding author:

Masayuki Sasaki, MD, PhD

Division of Medical Quantum Science,

Department of Health Sciences,

Graduate School of Medical Sciences,

Kyushu University,

3-1-1 Maidashi,

Higashi-ku,

Fukuoka 812-8582, Japan

Phone: +81-92-642-6746, Fax: +81-92-642-6723

E-mail: msasaki@hs.med.kyushu-u.ac.jp

Abstract

Objective

We aimed to evaluate the influence of the minimal misalignment of the hot spot on the repeatability of PET images using the repositioning of point sources.

Methods

Point sources with an inner-diameter of 1 mm were made with 1μL of ^{18}F solution. Seven point sources were placed on the x-axis in the field-of-view. For fixed position imaging, PET data were acquired for 10 min 5 times serially. For variable position imaging, PET data were acquired for 10 minutes each with the point sources placed at 0 mm, ±0.5 mm, and ±1.0 mm in the x-axis direction. The data were reconstructed using ordered-subsets expectation maximization (OSEM) and OSEM with point-spread function (OSEM+PSF) algorithms. The image matrix was 128×128, 200×200, 256×256, 400×400, and 512×512 pixels. The normalized maximum count (rMax), the variation of rMax (CV_{max}) and full width at half maximum (FWHM) were analyzed.

Results

The hot spots on OSEM images far from the center became faint and broad, while those on the OSEM+PSF images became small and dense. Although the rMax was overestimated

at the 5 cm position on OSEM image, those at other positions were overestimated on OSEM+PSF images with a matrix size of ≥256×256. The rMax showed a similar pattern in fixed and variable position images. The CV_{max} in fixed position OSEM images were <2%, irrespective of the matrix size. In contrast, the CV_{max} in variable position images were higher in comparison to fixed position images. The CV_{max} of the OSEM+PSF images were higher in comparison to OSEM images. The FWHM increased at positions far from the center on OSEM image, while that was stable at all positions on OSEM+PSF images.

Conclusion

The repeatability of the small hot spot was affected by the minimal misalignment, especially on the OSEM+PSF images. Precise positioning is necessary if PET is to be used as a biomarker. Professions should recognize that the PSF correction deteriorates the repeatability of the small hot spot although it improves the spatial resolution of PET images.

(344/350 words)

Key words: PET/CT, repeatability, repositioning, point-spread function

INTRODUCTION

^{18}F-fluoro-2-deoxy-D-glucose (FDG) positron emission tomography/computed tomography (PET/CT) is widely used for detection of tumors, staging, and monitoring of the responses to therapy and for prognostic stratification of various malignant tumors (*1-4*). The FDG-PET/CT images are often evaluated based on visual assessment and semi-quantitative values (*5-7*). Thus, the image quality and quantitative accuracy of PET images are important. However, numerous factors (*e.g.*, the acquisition time, patient body weight, dose of radiopharmaceuticals, and system characteristics) are known to affect the quantification of PET images (*8-10*). The two essential requirements for the quantification are the repeatability and reproducibility (*11*). Repeatability is defined as consistency in the results obtained in the same patient when they are examined multiple times using the same system. Reproducibility is defined as consistency in the results obtained in the same patient when they are examined on different systems in different institutions. Some studies have reported the repeatability and reproducibility of PET image quantification (*12,13*). Schwartz et al. evaluated the repeatability of SUV based on the statistical fluctuations using a cylindrical ^{68}Ge phantom and the flangeless Esser phantom filled with FDG (*14*). Doot et al. assessed repeatability and reproducibility using a National Electrical Manufactures

Association NU-2 Image Quality phantom that was removed and repositioned in the center of field-of-view, to approximately ±2 mm accuracy, 20 times, with three different PET scanners (*15*). They reported that the variation of the recovery coefficient using maximum count was 3.6%. The recent advancement of PET/CT technology has led to the increasing use FDG-PET/CT in the evaluation of sub-centimeter lesions (*16,17*). Repeatability is thus of increasing importance in the quantitative evaluation of small lesions; however, minimal misalignment, which cannot be avoided—even with careful repositioning—may have an impact on repeatability. Furthermore, a change in the physical constitution of the patient during clinical progress may change the positional relationship. Most studies have not examined the influence of minimal misalignment (≤2 mm) on the quantification of PET images.

The aim of the present study was to evaluate the influence of minimal misalignment of the hot spot on the repeatability of PET images using the repositioning of point sources.

MATERIALS AND METHODS

Point sources

The point sources consisted of a glass capillary (Microcaps, Drummond Scientific

Company, Broomall, PA, USA) of 51.8 mm in length and an inner-diameter of 0.99 mm. A glass capillary was filled with 1μL of ^{18}F solution (radioactivity: 76.5 MBq/mL). The length of the point source was approximately 1 mm. The radioactivity of the point source was measured using an automatic well γ-counter (AccuFLEX γ7001, Hitachi Aloka Medical, Ltd.) and was used as a reference value (true radioactivity; $C_{true,i}$, i=1~7). The mean C_{true} value of the for 7 sources was 29.0±1.69 kBq.

Positioning of point sources

The seven point sources were placed on the x-axis (intervals of 5 cm) in the field-of-view (Figure 1). The coordinates of the innermost point source in the field-of-view were 0 mm, 0 mm, while the coordinates of the outermost point source were 30 mm, 0 mm. For the fixed position images, data acquisition was performed for 10 minutes, 5 times serially. For the variable position images, the point sources were placed ±0.5 mm and ±1.0 mm in the x-axis direction to simulate the minimal of repositioning. Data acquisition was performed for 10 minutes each at above five positions. By using an automatic stage ALS-604-E1P (Chuo Precision Industrial Co., Ltd., Tokyo, Japan). The accuracy of the movement distance of point source was ±0.015 mm.

Data Acquisition

PET data were acquired using a PET/CT scanner (Biograph mCT, Siemens Healthcare). This PET scanner covers an axial field-of-view of 16.2 cm in length and a transaxial field-of-view of 70 cm in diameter. It consisted of a total of 24,336 lutetium orthosilicate detector elements (dimensions: of 4×4×20 mm). The coincidence time window was 4.1nsec. The PET data were acquired in a 3-dimensional list mode for 10 minutes. The full width at half maximum (FWHM) at 1 cm and 10 cm is 5.9 mm and 6.0 mm in standard processing (256×256) and 4.4 mm and 4.9 mm in high resolution processing (400×400), respectively.

Image Reconstruction

The PET images were reconstructed using the ordered-subset expectation maximization (OSEM) algorithm and that with point-spread function correction algorithm (OSEM+PSF). The parameters for both OSEM and OSEM+PSF were 3 iterations and 24 subsets. No post-smoothing filter was used for either algorithm. The image matrix was 128×128, 200×200, 256×256, 400×400, and 512×512 pixels (pixel sizes: 6.36, 4.07, 3.18, 2.04, and 1.59 mm, respectively). The slice thickness of the PET image was 5 mm. The CT data for

attenuation correction were obtained by a whole-body CT scan (parameters: 120 kV, 100 mA, 0.5-s tube rotation, and 5-mm slice). Scatter correction was performed using the model-base method.

Data Analysis

We placed a circular region of interest (ROI*i*, *i*=1~7) to include the whole radioactivity of each point source. The maximum radioactivity of the point source "*i*" was measured as $C_{max,i}$. Because the radioactivity of the seven point sources was not completely equal, $C_{max,i}$ was normalized by $C_{true,i}$ as $rMax_i$.

$$rMax_i = C_{max,i} / C_{true,i}$$

The variation of $rMax_i$ was evaluated by the coefficient of variance (CV_{max}), which was calculated as follows:

$$CV_{max,i} = \text{standard deviation of } rMax_i / \text{mean of } rMax_i \times 100\ [\%]$$

The FWHM of x-direction on point source "*i*" was calculated as $FWHM_i$, according to the National Electrical Manufactures Association requirements (NEMA-NU2-2012) (*18)*. The maximum pixel value and its two nearest-neighbor points were used for a parabolic fitting. The position at half of the maximum value was determined by linear interpolation

between adjacent pixels. The pixel size was set to 6.36, 4.07, 3.18, 2.04, and 1.59 mm, respectively.

RESULTS

Figure 2 shows images of the point source at a fixed position that were obtained using the OSEM and OSEM+PSF. The shape and density of the hot spots differed according to the position and the matrix size. The images of point sources far from the center became faint and broad. In images with large matrix sizes, they were dense and sharp. In comparison to the OSEM images, the hot spots on the OSEM+PSF images were small and dense. Figure 3 shows the point source in variable position images with a 400×400 matrix size that were obtained using the OSEM and OSEM+PSF. The hot spots located far from the center also appeared faint and broad, similar to the fixed position images. The density and shape of the hot spots differed according to the positions of the point source. In comparison to the OSEM images, the hot spots on the OSEM+PSF images were small and dense.

Figure 4 shows the $rMax_i$ values for both the fixed and variable positions. On the OSEM images, the $rMax_i$ values of most point sources at both positions were underestimated

(range: 0.58 to 0.13) in images with a matrix size of ≤200×200. In contrast, the $rMax_i$ was overestimated as 1.37 at the 5 cm position in images with a matrix size of ≥256×256. The $rMax_2$ value was the highest at 5 cm and gradually decreased as along with the distance from the center increased. The $rMax_i$ values in the fixed and variable positions showed a similar pattern. Table 1 shows the $CV_{max,i}$ values for fixed and variable position OSEM images. In the fixed position, the $CV_{max,i}$ values were <2%, irrespective of the matrix size (range: 0.28% to 1.73%). In contrast, the $CV_{max,i}$ values of the variable position images were higher in comparison to the fixed position images (range 0.64% to 12.5%).

The $rMax_i$ values of the OSEM+PSF images were higher in comparison to the OSEM images (Figure 4). The $rMax_2$ was the highest at 5 cm with a matrix size of ≥256×256. The $rMax_i$ value showed a similar pattern in fixed and variable position images. Table 2 shows the $CV_{max,i}$ values of OSEM+PSF images. The $CV_{max,i}$ values of the PSF images were higher in comparison to the OSEM images. In the fixed position images, the $CV_{max,i}$ values were ≤2.76%, irrespective of the matrix size (range 0.33% to 2.76%). In contrast, the $CV_{max,i}$ values of the variable position images were higher than those of the fixed position images (range: 0.92% to 31.7%). High $CV_{max,i}$ values were observed irrespective of the matrix size.

Figure 5 shows the $FWHM_i$ values of the fixed and variable position images. The $FWHM_i$ increased at positions located far from the center in OSEM images, especially in images with a matrix size of 128×128. In contrast, the $FWHM_i$ values of the OSEM+PSF images were stable in all positions. The $FWHM_i$ was large in images with small matrix sizes. The $FWHM_i$ values of the fixed and variable position images showed a similar pattern.

DISCUSSION

We examined the influence of minimal misalignment through simulated repositioning on the repeatability of PET images. The maximum counts were different and varied according to the position and matrix size. The degree of variation in the variable position images was larger than in the fixed position images. In particular, the degree of variation of the OSEM+PSF images was higher in comparison to that of the OSEM images. The FWHM values of OSEM images increased at positions located far from the center, while the FWHM values of OSEM+PSF images were stable at all positions.

The intensity and shape of point source images differed according to the position and matrix size. Additionally, the $CV_{max,i}$ values of the variable position images were higher

than the values of the fixed position images. The measurements of the radioactivity of a small region are strongly affected by the partial volume effect (*19*). Mansor et al. reported that the precision of SUV_{max} was affected by phantom repositioning in a phantom study that used a hot sphere of ≤15 mm in diameter (*20*). Furthermore, Adams et al. reported that the measured PET count varied and that there was a relationship between the alignment of the hot spot and the pixels (*21*). The PET count varied and was underestimated if the hot spot was located between some pixels due to the partial volume effect (*19*). The alignment of the point source in a pixel is considered to influence the height and shape of the point-spread function.

The $CV_{max,i}$s values of the fixed position images were <3% in the study. Schwartz et al. reported that statistical variation in the order of 5% (*14*). Thus, the variation of the maximum count of the fixed position images in present study was considered to have resulted from the statistical variation. On the other hand, the $CV_{max,i}$ values of the variable position OSEM images ranged from 0.64% to 12.5% in the present study. Some patient studies have reported that the test-retest SUV variability was approximately 10-15% (*13, 22, 23*). Doot et al. reported that the SUV variability without any biological variability in a repositioning study (imaging protocol variation: <10%) using a National Electrical

Manufactures Association NU-2 IQ phantom (*15*). Thus, the $CV_{max,i}$ values of the variable position images are considered to be an important exacerbating factor for repeatability.

The $rMax_i$ and $CV_{max.}$ values of the OSEM+PSF images were higher in comparison to those of the OSEM images. PSF correction has been used to improve the spatial resolution of PET images. The $FWHM_i$ values increased at positions located far from the center of OSEM images, while those of PSF images were stable at all positions. Murata et al. also showed that the PSF correction reduced the dependency of the spatial resolution on the position (*24*). PSF correction has been reported to the result in overestimation due to edge artifacts in small regions, and is therefore a problem for quantification (*25*). We previously reported that the edge artifacts were observed as a sharp peak at the center of small hot spheres (*26*). Zhang et al. found that edge artifacts were unclear in areas of low radioactivity (*27*). Thus, the degree of overestimation due to edge artifacts varied according to the level of radioactivity. Furthermore, PSF correction was reported to increase SUV variability in a phantom study (*20*). Although PSF correction improved the PET image quality, OSEM+PSF images are considered to increase the variation of the $rMax_i$ and $CV_{max,i}$ values in comparison to OSEM images.

The present study is associated with several limitations. First, the precise positional

relationship between the point source and the pixel could not be clarified. A simulation study may solve this problem. Second, the FWHM values were estimated by parabolic fitting based on the nearest pixel values. The FWHM value might be overestimated in images with large pixels. Third, we evaluated the repeatability of PET/CT images using a point source in air. Because lesions in the human body are usually located in areas with the physical uptake of radioactivity, a further study that also investigates background radioactivity should be performed.

CONCLUSION

The repeatability of small hot spot images was affected by the minimal misalignment (≤2 mm) especially on images reconstructed with the PSF algorithm. Positioning is considered to be an important factor if PET examinations are to be used as a reliable biomarker. Professions should recognize that the PSF correction deteriorates the repeatability of the small hot spot although it improves the spatial resolution of PET images.

Acknowledgement

The authors declare no conflicts of interest in association with the present study.

References

1. Rohren EM, Turkington TG, Coleman RE. Clinical applications of PET in oncology. *Radiology*. 2004;231:305-332.

2. Hicks RJ. Role of ^{18}F-FDG PET in assessment of response in non-small cell lung cancer. *J Nucl Med*. 2009;50(suppl 1):31S-42S.

3. Fischer B, Lassen U, Mortensen J, et al. Preoperative staging of lung cancer with combined PET-CT. *N Engl J Med*. 2009;361:32-39.

4. van Elmpt W, Ollers M, Dingemans AM, Lambin P, De Ruysscher D. Response assessment using ^{18}F-FDG PET early in the course of radiotherapy correlates with survival in advanced stage non-small cell lung cancer. *J Nucl Med*. 2012;53(10):1514-1520.

5. Young H, Baum R, Cremerius U, et al. Measurement of clinical and subclinical tumor response using [^{18}F]-fluorodeoxyglucose and positron emission tomography: review and 1999 EORTC recommendations. European Organization for Research and Treatment of Cancer (EORTC) PET Study Group. *Eur J Cancer.* 1999;35(13):1773-1782.

6. Wahl RL, Jacene H, Kasamon Y, Lodge MA. From RECIST to PERCIST: Evolving

Considerations for PET response criteria in solid tumors. *J Nucl Med*. 2009;50(suppl 1):122S-150S.

7. Weber WA, Petersen V, Schmidt B, et al. Positron emission tomography in non-small-cell lung cancer: prediction of response to chemotherapy by quantitative assessment of glucose use. *J Clin Oncol*. 2003;21:2651-2657.
8. Keyes JW Jr. SUV: standard uptake or silly useless value? *J Nucl Med.* 1995;36(10):1836-1839.
9. Westerterp M, Pruim J, Oyen W, et al. Quantification of FDG PET studies using standardised uptake values in multi-centre trials: effects of image reconstruction, resolution and ROI definition parameters. *Eur J Nucl Med Mol Imaging*. 2007;34(3):392-404.
10. Boellaad R. Standards for PET image acquisition and quantitative data analysis. *J Nucl Med.* 2009;50(suppl 1):11S-20S.
11. Boellaard R, Delgado-Bolton R, Oyen WJ, et al. FDG PET/CT: EANM procedure guidelines for tumor imaging: version 2.0. *Eur J Nucl Med Mol Imaging.* 2015;42:328-354.
12. Minn H, Zasadny KR, Quint LE, Wahl RL. Lung cancer: reproducibility of quantitative

measurements for evaluating 2-[F-18]-fluoro-2-deoxy-D-glucose uptake at PET. *Radiology*. 1995;196:167-173.

13. Velasquez LM, Boellaard R, Kollia G, et al. Repeatability of ^{18}F-FDG PET in a multicenter phase 1 study of patients with advanced gastrointestinal malignancies. *J Nucl Med*. 2009;50:1646-1654.
14. Schwartz J, Humm JL, Gonen M, et al. Repeatability of SUV measurements in serial PET. *Med Phys*. 2011;38:2629-2638.
15. Doot RK, Scheuermann JS, Christian PE, Karp JS, Kinahan PE. Instrumentation factors affecting variance and bias of quantifying tracer uptake with PET/CT. *Med Phys*. 2010;37:6035-6046.
16. Yoon HJ, Lee JJ, Kim YK, Kim SE. FDG-PET/CT is superior to enhanced CT in detecting recurrent subcentimeter lesions in the abdomeninopelvic cavity in colorectal cancer. *Nucl Med Mol Imaging*. 2011;45:132-138.
17. Kunawudhi A, Pak-art R, Keelawat S, Tepmongkol S. Detection of subcentimeter metastatic cervical lymph node by ^{18}F-FDG PET/CT in patients with well-differentiated thyroid carcinoma and high serum thyroglobulin but negative ^{131}I whole-body scan. *Clin Nucl Med*. 2012;37:561-567.

18. National Electrical Manufactures Association. NEMA standards publication NU 2-2012: performance measurements of positron emission tomographs. Rosslyn: National Electrical Manufactures Association; 2012.

19. Soret M, Bacharach SL, Buvat I. Partial-volume effect in PET tumor imaging. *J Nucl Med.* 2007;48:932-945.

20. Mansor S, Pfaehler E, Heijtel D, Lodge MA, Boellaard R, Yaqub M. Impact of PET/CT system, reconstruction protocol, data analysis method and repositioning on PET/CT precision: an experimental evaluation using an oncology and brain phantom. *Med Phys.* 2017;44:6413-6424.

21. Adams MC, Turkington TG, Wilson JM, Wong TZ. A systematic review of the factors affecting accuracy of SUV measurements. *AJR Am J Roentgenol*. 2010;195:310-320.

22. Weber WA, Gatsonis CA, Mozley PD et al. Repeatability of ^{18}F-FDG PET/CT in advanced non-small cell lung cancer: prospective assessment in 2 multicenter trials. *J Nucl Med.* 2015:56;1137-1143.

23. Kramer GM, FringsV, Hoetjes N, et al. Repeatability of quantitative whole-body ^{18}F-FDG PET/CT uptake measures as function of uptake interval and lesion selection in no-small cell lung cancer patients. *J Nucl Med.* 2016;57:1343-1349.

24. Murata T, Miwa K, Miyaji N, et al. Evaluation of spatial dependence of point spread function-based PET reconstruction using a traceable point-like ^{22}Na source. *EJNMMI Phys*. 2016;3:26.

25. Snyder DL, Miller MI, Thomas LJ, Politte DG. Noise and edge artifacts in maximum-likelihood reconstructions for emission tomography. *IEEE Trans Med Imaging*. 1987;6:228-238.

26. Kidera D, Kihara K, Akamatsu G, et al. The edge artifact in point-spread function-based PET reconstruction at different sphere-to-background ratios of radioactivity. *Ann Nucl Med*. 2016;30:97-103.

27. Zhang L, Staelens S, Van Holen R, Verhaeghe J, Vandenberghe S. Characterization of the ringing artifacts in rotator-based reconstruction with Monte Carlo-based resolution compensation for PET. *Med Phys*. 2010;37:4648-4660.

FIGURE LEGENDS

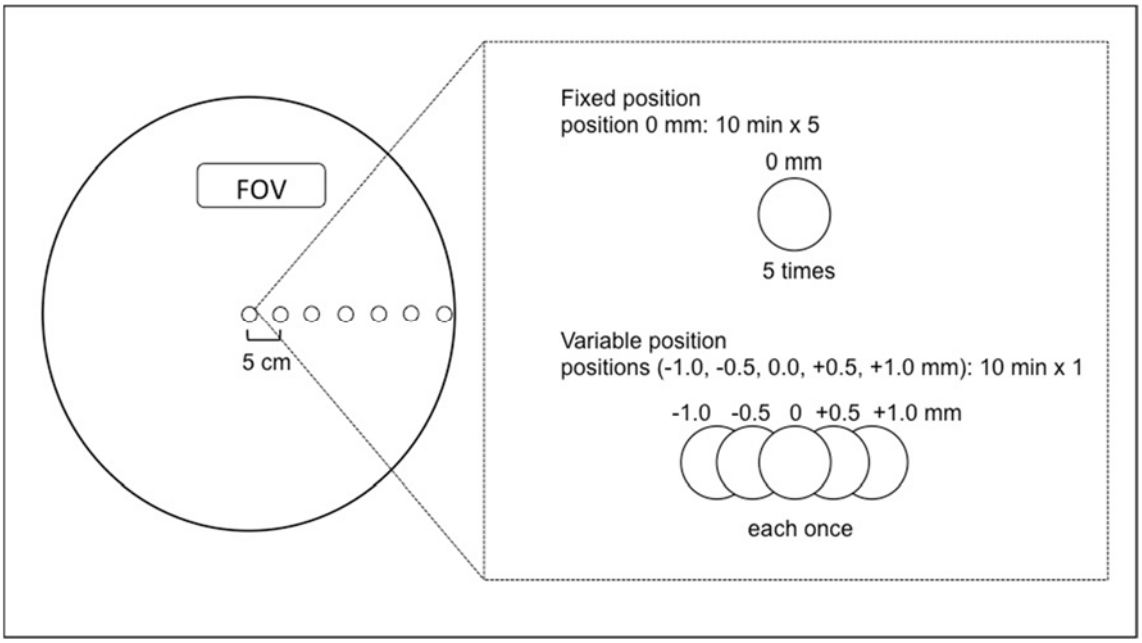

Figure 1. The setting of the point sources. Seven point sources were placed on the x-axis (interval: 5 cm). For the fixed position images, data acquisition was performed for 10 minutes, 5 times serially. For the variable position images, data acquisition was performed for 10 minutes each with the point sources placed at 0 mm, ±0.5 mm, and ±1.0 mm in the x-axis direction to simulate the minimal of repositioning.

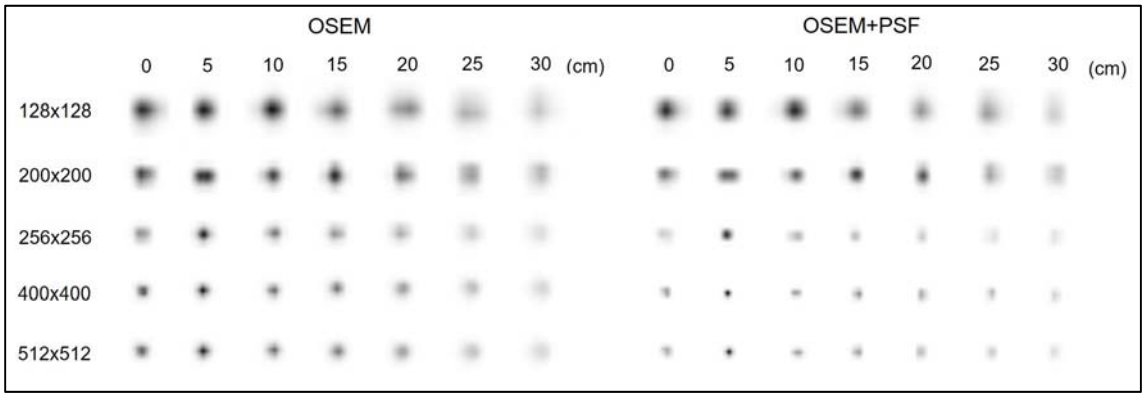

Figure 2. Images of the point sources at a fixed position reconstructed by OSEM and OSEM+PSF with 5 different matrix sizes. The images of point sources far from the center became faint and broad. The hot spots on the OSEM+PSF images were smaller and denser than those on the OSEM image. (OSEM; ordered-subset expectation maximization algorithm, OSEM+PSF; OSEM with point-spread function correction algorithm).

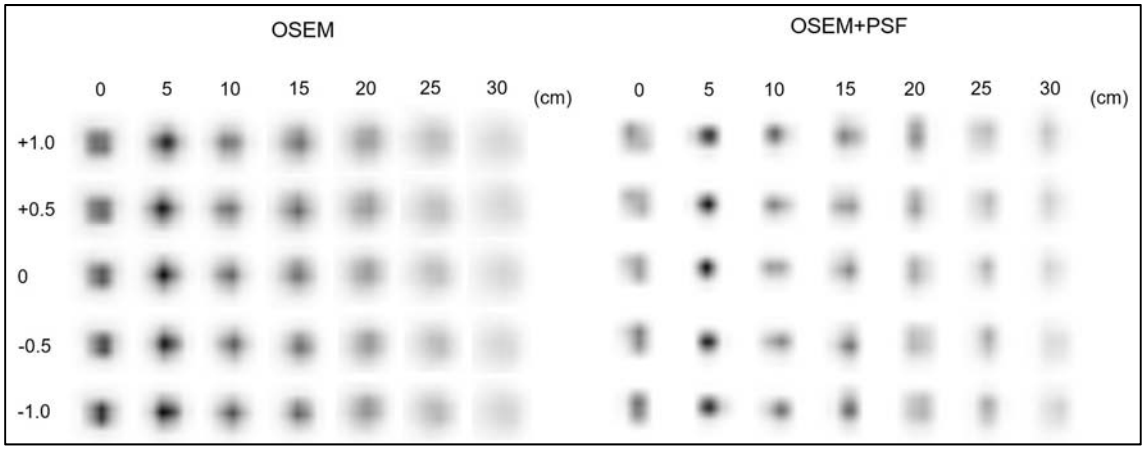

Figure 3. The images of point sources at variable positions reconstructed by OSEM and OSEM+PSF with a matrix size of 400×400. The density and shape of the point sources differed among the positions. (OSEM; ordered-subset expectation maximization algorithm, OSEM+PSF; OSEM with point-spread function correction algorithm).

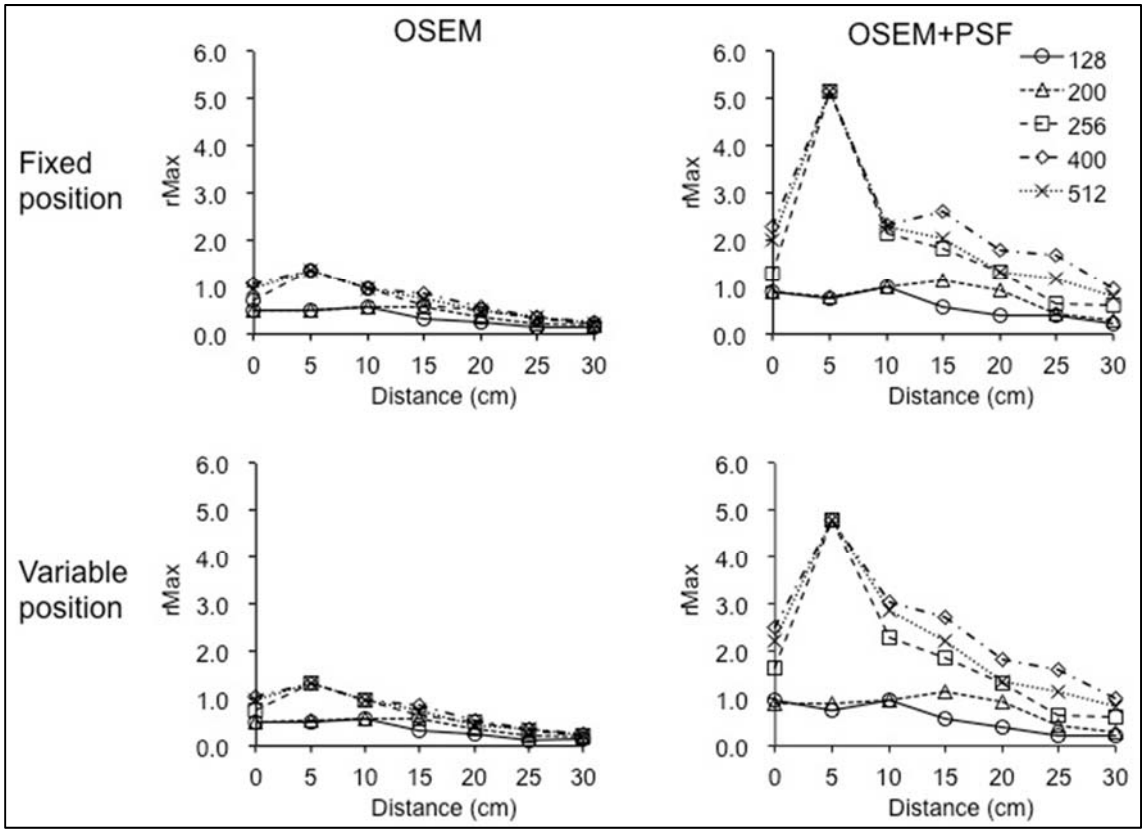

Figure 4. The $rMax_{,i}$ values at both fixed and variable positions on OSEM and OSEM+PSF images. At both positions, the $rMax_{,i}$ values decreased at positions far from the center. The $rMax_{,i}$ values on OSEM+PSF images were higher than those on OSEM images. (OSEM; ordered-subset expectation maximization algorithm, OSEM+PSF; OSEM with point-spread function correction algorithm, $rMax_i$; normalized maximum count of ROI_i that is the ratio of measured maximum count and true radioactivity count).

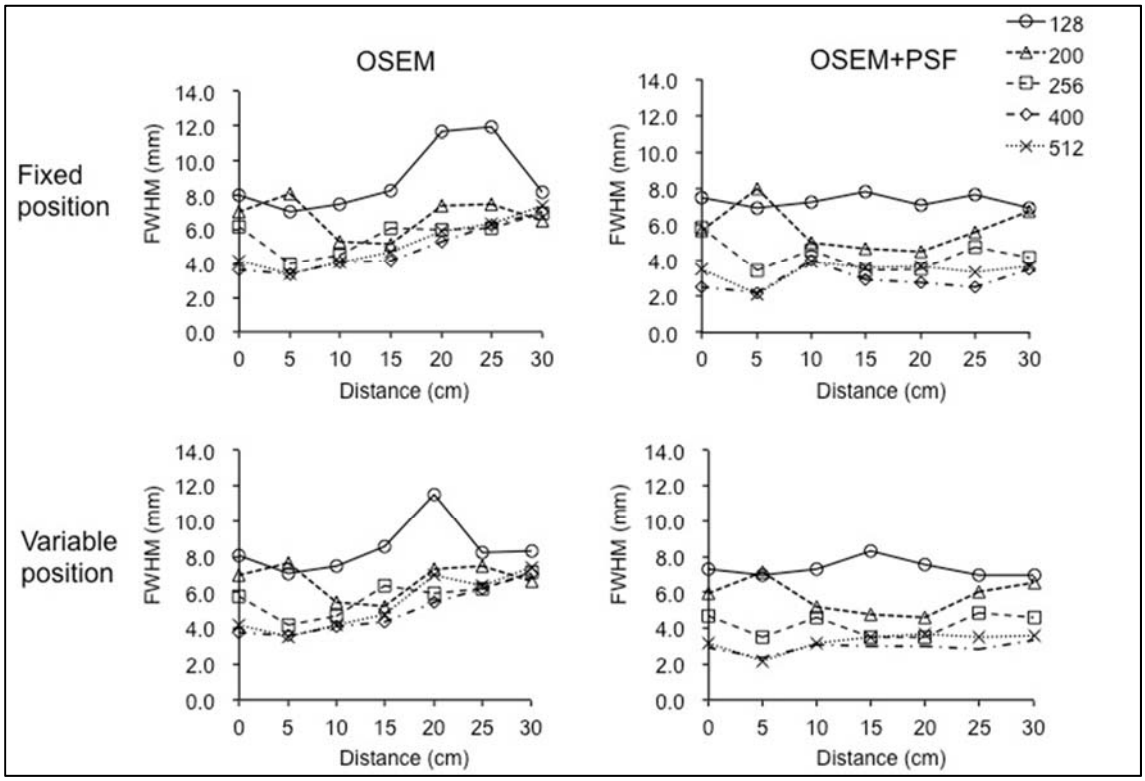

Figure 5. The $FWHM_{,i}$ values at both fixed and variable position on OSEM and OSEM+PSF images. The $FWHM_{,i}$ values increased at positions far from the center on OSEM images. The $FWHM_{,i}$ values of OSEM+PSF images were stable at all positions. (OSEM; ordered-subset expectation maximization algorithm, OSEM+PSF; OSEM with point-spread function correction algorithm, $FWHM_i$; full width at half maximum of ROI_i).

TABLES

Table 1. The $CV_{max,i}$ values on OSEM images.

Matrix size		position [cm]						
		0	5	10	15	20	25	30
128×128	Fixed	0.39%	0.31%	0.31%	0.56%	1.30%	1.03%	0.52%
	Variable	7.06%	0.70%	3.68%	4.90%	12.5%	11.1%	5.40%
200×200	Fixed	0.39%	0.49%	0.31%	0.49%	0.32%	1.04%	1.02%
	Variable	7.06%	5.84%	3.68%	0.64%	7.80%	5.61%	1.86%
256×256	Fixed	0.69%	0.67%	0.46%	0.75%	0.41%	0.88%	1.73%
	Variable	10.9%	3.91%	7.68%	6.35%	5.48%	1.14%	3.17%
400×400	Fixed	0.49%	0.67%	0.46%	0.98%	0.87%	0.84%	1.18%
	Variable	9.13%	3.91%	5.96%	2.58%	2.38%	1.60%	3.29%
512×512	Fixed	0.28%	0.67%	0.46%	0.85%	0.80%	0.31%	0.68%
	Variable	4.81%	3.91%	6.31%	1.71%	2.07%	0.75%	2.46%

$CV_{max,i}$; the coefficient of variance of noemalized maximum count ($rMax_i$).

Table 2. The $CV_{max,i}$ values on OSEM+PSF images.

Matrix size		position [cm]						
		0	5	10	15	20	25	30
128×128	fixed	0.44%	0.84%	0.56%	0.47%	0.33%	1.22%	1.39%
	variable	9.89%	0.92%	10.4%	7.09%	6.83%	18.7%	5.76%
200×200	fixed	0.46%	0.85%	0.50%	0.57%	0.30%	1.09%	1.32%
	variable	9.89%	10.21%	10.4%	7.09%	6.64%	18.7%	10.89%
256×256	fixed	1.55%	0.73%	0.84%	1.00%	1.04%	1.99%	0.92%
	variable	25.1%	5.47%	31.7%	6.97%	5.66%	8.85%	22.1%
400×400	fixed	1.27%	0.73%	0.49%	1.48%	0.69%	2.76%	1.39%
	variable	18.8%	5.47%	16.3%	16.6%	21.0%	14.8%	13.9%
512×512	fixed	0.39%	0.73%	0.41%	1.48%	1.04%	0.88%	1.03%
	variable	12.4%	5.47%	13.7%	12.3%	10.3%	5.33%	12.6%

$CV_{max,i}$; the coefficient of variance of normalized maximum count ($rMax_i$).